Signal Estimation for UAV Control Loop Identification Using Artificial Immune Systems

H. B. Rezende*, M. F. Silva†, M. F. Santos‡, L. M. Honório§, L. A. Z. Silva¶,
V. F. Vidal‖, J. M. S. Ribeiro**, A. S. Cerqueira††, A. A. N. Pancoti‡‡, B. A. Regina[x]

Juiz de Fora Federal University,
UFJF, Juiz de Fora, MG, 36036-900, Brazil
henrique.rezende@engenharia.ufjf.br*, mathaus.silva@engenharia.ufjf.br†, leonardo.honorio@ufjf.edu.br§,
luiz.zillmann@engenharia.ufjf.br¶ vinicius.vidal@engenharia.ufjf.br‖, joao.ribeiro@engenharia.ufjf.br**,
augusto.santiago@ufjf.edu.br††, antonio.pancoti@engenharia.ufjf.br‡‡, almeida.bruno@engenharia.ufjf.br[x]

Centro Federal de Educação Tecnológica de Minas Gerais,
CEFET-MG, Leopoldina, MG, 36700-000, Brazil
murillo@leopoldina.cefetmg.br‡

***Abstract*—The paper aims to estimate a signal that best provides the identification of a quadrotor type Unmanned Aerial Vehicle angular control loop using a bioinspired metaheuristic Artificial Immune System algorithm. The angular control loop was approximated by a second-order system using the Recursive Least Square method. The results were satisfactory, presenting, in general, a rich enough signal to provide a correct estimation of the system.**

***Keywords*—Optimization, Artificial Immune System, Recursive Least Square Method, Quadrotors.**

I. Introduction

Metaheuristic optimization algorithms, like Genetic Algorithms (GA), Simulated Annealing (SA), Artificial Bee Colony (ABC), Ant Colony Algorithms (AC), and Artificial Immune Systems (AIS) are being used for different problems. Methods such as those mentioned have been the focus of research and improvements, showing a more efficient performance than conventional optimization techniques, despite presenting some limitations depending on its application [1]–[3].

AIS algorithms are inspired by the immune system [4]. A set of AIS algorithms has been developed since the early 1990s by independent groups, having different properties and suitability for a diverse set of applications. The obtained results, in many cases, have rivalled or improved statistical learning techniques and some machine learning [5].

Over the years, several reviews about AIS have been made. In general, Negative Selection Algorithm [6], Clonal Selection Algorithm [7], and Immune Network Algorithm are the base algorithms of the majority of AIS techniques [8].

The AIS technique has been widely used in several fields, such as data analysis [9]–[11]; optimization of multiobjective functions [12]–[14]; dynamic polymorphic agents scheduling and execution [15]; solution of optimal power flow problems [16]; and error detection [17]–[20]. This algorithm have a large capacity of robust data processing for complex problems solution [4].

Regarding signal and parameter estimation, a vast number of papers have been developed, such as parameter estimation in dynamic systems through optimal input signals [21]; identification of multi-input systems [22]; and optimal parameter estimation of constrained nonlinear dynamical systems using persistently-exciting signal generation [23].

The use of Unmanned Aerial Vehicles (UAV), more specifically, the quadrotor type, is exponentially growing in many fields, as military, research, and commercial [24]. The expansion is due to the improvement in the quality of sensors and electronic equipment, as well as the number of developers working in this area [25].

Based on the AIS optimization technique, this paper aims to estimate a suitable input signal capable of approaching a system for a second-order transfer function using Recursive Least Squares (RLS) technique, as well as applying to the control loops present on quadrotors.

II. Artificial Immune Systems

The AIS is an algorithm created from observations of bio-immune systems [26]. This technique is inspired by the immune response of organisms consisting of the identification of antigens by B-cells (lymphocytes), which after their recognition produce antibodies to fight them. Antigens are the foreign bodies that attack organisms, and B-cells are defense cells [4].

The immune system must distinguish between elements belonging to the organism (proper) and foreign elements (improper), which have to be recognized by lymphocytes. However, not every B-cell has a binding affinity with a given antigen. Thus, there are thousands of different B-cells seeking this recognition. When the recognition is achieved, the B-cell is cloned to try to fight the antigen and mutates to try to find a lymphocyte with even higher affinity [27].

The organism has a vast diversity of lymphocytes, inherited genes, which function as a library providing random recom-

978-1-5386-4444-7/18/$31.00 ©2018 IEEE

bination and generating new lymphocytes that may have high affinity with the antigen of the systems [27].

Mathematical equations can be used to express the functioning of the immune system. In (1) is calculated the number of clones to be generated for solutions with higher degrees of affinity. In (2), the solution affinity value is normalized to be applied in (3), which expresses the mutation probability of a given solution.

$$Nc_i = \text{round}(\frac{c.N}{i}) \tag{1}$$

$$Fn_i = \frac{Fi}{Fi\max} \tag{2}$$

$$\alpha_i = e^{-h.\,Fn_i} \text{ (Maximization)} \tag{3}$$

or

$$\alpha_i = e^{\frac{-h}{Fn_i}} \text{ (Minimization)}$$

where:

Nc_i = number of clones of solution i.
c = cloning process control constant.
N = number of solution possibilities.
Fn_i = normalized affinity value of solution i.
Fi = affinity value of solution i.
Fi_{Max} = highest affinity value among the solutions.
α_i = clone mutation probability.
h = affinity maturation process control constant.

III. Methodology

The methodology used in this work consists of quadrotor modelling and control presentation; RLS technique use for estimation of the desired transfer function; AIS technique implementation; results acquisition.

A. Non-Linear Aircraft Modelling and Control

Some UAV physical properties are measured in $\mathcal{F}^I$ (roll, pitch and yaw angles, angular velocities), while some properties are measured in $\mathcal{F}^b$ (linear accelerations).

Typically, UAV modelling uses the following state variables: the vector $[p_n, p_e, h]^T$ represents the inertial North, East and Altitude (facing down) positions along the $(\hat{i}^i, \hat{j}^i, -\hat{k}^i)$ axes representing the inertial frame; the vector $[\phi, \theta, \psi]^T$ represents the roll, pitch and yaw angles considering the vehicle frame $(\hat{i}^v, \hat{j}^v, -\hat{k}^v)$. The vectors $[u, v, \omega]^T$ and $[p, q, r]^T$ represent the three dimensional speeds and angular velocities over the axes $(\hat{i}^b, \hat{j}^b, -\hat{k}^b)$ of the body frame [28], [29].

Its position $\boldsymbol{\eta} \in \mathbb{R}^6$ is the generalized position with vector $\boldsymbol{\eta_1} \in \mathbb{R}^3$ between origins of $\mathcal{F}^I$ and $\mathcal{F}^b$, while $\boldsymbol{\eta_2} \in \mathbb{R}^3$ is defined with the orientation of $\mathcal{F}^b$ with the respect to the $\mathcal{F}^I$. The orientation is defined with three consecutive rotations around the $\mathcal{F}^I$ coordinate axes, roll-pitch-yaw order. According to [30], (4) presents the default nomenclature.

$$\begin{aligned} \boldsymbol{\eta_1} &= [p_n \;\; p_e \;\; h]^T \\ \boldsymbol{\eta_2} &= [\phi \;\; \theta \;\; \psi]^T \\ \boldsymbol{\eta} &= [\boldsymbol{\eta_1} \;\; \boldsymbol{\eta_2}]^T \end{aligned} \tag{4}$$

Regarding to velocities, (5) presents them:

$$\begin{aligned} \boldsymbol{\nu_1} &= [\boldsymbol{v^b}] = [u \;\; v \;\; w]^T \\ \boldsymbol{\nu_2} &= [\boldsymbol{\omega^b}] = [p \;\; q \;\; r]^T \\ \boldsymbol{\nu} &= [\boldsymbol{\nu_1} \;\; \boldsymbol{\nu_2}]^T \end{aligned} \tag{5}$$

where $\boldsymbol{\nu} \in \mathbb{R}^6$ is the generalized velocity vector, $\boldsymbol{\nu_1} \in \mathbb{R}^3$ is the linear velocity vector, $\boldsymbol{\nu_2} \in \mathbb{R}^3$ is the angular velocity vector, both in $\mathcal{F}^b$.

The 6 Degrees of Freedom (DOFs) rigid body kinematics and dynamics model is expressed in (6).

$$\dot{\boldsymbol{\eta}} = \boldsymbol{J}\boldsymbol{\nu} \tag{6}$$

where $\dot{\boldsymbol{\eta}} \in \mathbb{R}^6$ is the generalized velocity vector in $\mathcal{F}^I$ and $\boldsymbol{J} \in \mathbb{R}^{6\times6}$ is the generalized rotation and transformation matrix, presented below [31]:

$$\boldsymbol{J} = \begin{bmatrix} \boldsymbol{J_1} & \boldsymbol{0_{3\times3}} \\ \boldsymbol{0_{3\times3}} & \boldsymbol{J_2} \end{bmatrix} \tag{7}$$

$$\boldsymbol{J_1} = \begin{bmatrix} c\theta c\psi & s\phi s\theta c\psi - c\theta s\psi & c\phi s\theta c\psi + s\phi s\psi \\ c\theta s\psi & s\phi s\theta s\psi + c\phi c\psi & c\phi s\theta s\psi - s\phi c\psi \\ -s\theta & s\phi s\theta & c\phi c\theta \end{bmatrix} \tag{8}$$

$$\boldsymbol{J_2} = \begin{bmatrix} 1 & s\phi t\theta & c\phi t\theta \\ 0 & c\phi & -s\phi \\ 0 & s\phi/c\theta & c\phi/c\theta \end{bmatrix} \tag{9}$$

where $c\theta \triangleq \cos\theta$, $s\theta \triangleq \sin\theta$, $t\theta \triangleq \tan\theta$, $\boldsymbol{J_1} \in \mathbb{R}^{3\times3}$ is the rotation matrix to relate linear velocity vector and $\boldsymbol{J_2} \in \mathbb{R}^{3\times3}$ is the rotation matrix to relate angular velocity vector, both from $\mathcal{F}^b$ to $\mathcal{F}^I$.

UAV dynamics are described by differential equations from Newton-Euler method. The mass m and the body inertia matrix $\boldsymbol{I_{CG}}$ are taken into consideration in the 6 DOFs rigid body, as shown in (10).

$$\boldsymbol{M_b}\dot{\boldsymbol{\nu}} + \boldsymbol{C_b}(\boldsymbol{\nu})\boldsymbol{\nu} = \boldsymbol{\tau} \tag{10}$$

where:

$$\boldsymbol{M_b} = \begin{bmatrix} m\boldsymbol{I} & \boldsymbol{0_{3\times3}} \\ \boldsymbol{0_{3\times3}} & \boldsymbol{I_{CG}} \end{bmatrix} \tag{11}$$

$$\boldsymbol{C_b}(\boldsymbol{\nu}) = \begin{bmatrix} m\boldsymbol{S}(\boldsymbol{\nu_2}) & \boldsymbol{0_{3\times3}} \\ \boldsymbol{0_{3\times3}} & -\boldsymbol{S}(\boldsymbol{I_{CG}}\boldsymbol{\nu_2}) \end{bmatrix} \tag{12}$$

$$\boldsymbol{\tau} = \boldsymbol{\tau^p} + \boldsymbol{\tau^g} \tag{13}$$

where $\boldsymbol{M_b} \in \mathbb{R}^{6\times6}$ is the system inertia matrix, $\boldsymbol{C_b}(\boldsymbol{\nu}) \in \mathbb{R}^{6\times6}$ is the Coriolis-centripetal matrix at the body-fixed frame $\mathcal{F}^b$, $\boldsymbol{S}(\boldsymbol{\nu_2}) \in \mathbb{R}^{3\times3}$ is the skew-symmetrical matrix of vector $\boldsymbol{\nu_2}$, $\boldsymbol{\tau} = [\tau_x, \tau_y, \tau_z, \tau_\phi, \tau_\theta, \tau_\psi] \in \mathbb{R}^6$ is resultant vector compound

by vector of Gravitational $\boldsymbol{\tau^g} \in \mathbb{R}^6$ and Propulsion $\boldsymbol{\tau^p} \in \mathbb{R}^6$ forces and torques, both in the body-fixed frame $\mathcal{F}^b$. Note that $\boldsymbol{I} \in \mathbb{R}^{3\times3}$ is the identity matrix, different from $\boldsymbol{I_{CG}}$.

Considering the constructive symmetry characteristics, (14) presents the body inertia matrix $\boldsymbol{I_{CG}}$.

$$\boldsymbol{I_{CG}} = \begin{bmatrix} I_{xx} & 0 & 0 \\ 0 & I_{yy} & 0 \\ 0 & 0 & I_{zz} \end{bmatrix} = \begin{bmatrix} 0.0188 & 0 & 0 \\ 0 & 0.0188 & 0 \\ 0 & 0 & 0.0319 \end{bmatrix} \tag{14}$$

Concerning propulsion forces and gravitational forces and torques, (15) presents them.

$$\boldsymbol{\tau} = \begin{pmatrix} \boldsymbol{J_1}^{\boldsymbol{T}} \\ \boldsymbol{0_{3\times3}} \end{pmatrix} \begin{pmatrix} 0 \\ 0 \\ mg \end{pmatrix} + \begin{pmatrix} 0 \\ 0 \\ -k_1\delta_1 - k_1\delta_2 - k_1\delta_3 - k_1\delta_4 \\ A_1 \\ A_2 \\ A_3 \end{pmatrix} \tag{15}$$

where δ_* is the PWM (Pulse Width Modulation) control signal of the respective propulsion motor (from 1 to 4) and g is the gravitational constant.

Now it is necessary to do some linearization of this full non-linear model to use this linear function to estimate its parameters. It is important to highlight that its evaluation will be done by taking the full model into account.

Following the methodology presented in [32] and [33], it is possible to approach the equations for small angles and assume that, because of small angle variations, Coriolis terms (qr, pr and pq) are small. Then, (16) express the simplified three angular model:

$$\begin{bmatrix} \ddot{\phi} \\ \ddot{\theta} \\ \ddot{\psi} \end{bmatrix} = \begin{bmatrix} \tau_\phi / I_{xx} \\ \tau_\theta / I_{yy} \\ \tau_\psi / I_{zz} \end{bmatrix} \tag{16}$$

The design of PID controller gains (K_P, K_I, and K_D) is performed with the intention of producing responses in the angular attitude control meshes as presented in (17).

$$G(s) = \frac{\omega_n^2}{s^2 + 2\zeta\omega_n s + \omega_n^2} \tag{17}$$

where ω_n is the desired natural frequency and ζ is the desired damping ratio.

More details about UAV modeling and its simplification procedures are found in the related works [24], [32], [34]–[36].

B. Recursive Least Square Method

Recursive Least Squares estimation consists in the formation of normal equations based on data that describe the linearized relationship between residual measures and estimation parameters [37].

Through the elimination technique, normal equations can be solved by parameter estimation. In addition, the covariance matrix can be obtained by inverting the matrix of normal equations. In other words, the usual method for matrix inversion is susceptible to numerical errors [38].

Thus, (18) is the expression that allows error minimization through the RLS technique.

$$\min_x \frac{1}{2}||\mathcal{M}x - D||_2^2 \tag{18}$$

where *x* are the variables to be estimated; *M* is the response input matrix of the function to be estimated and *D* the respective output matrix.

From this assumption, the presented matrices must be obtained. Initially, for purposes of robustness in the method, a generic second-order transfer function was considered as a result of the function estimated by the RLS, presented in (19).

$$G(s) = \frac{Y(s)}{X(s)} = \frac{A_2 s^2 + A_1 s + A_0}{B_2 s^2 + B_1 s + 1} \tag{19}$$

where A_2, A_1, A_0, B_2, and B_1 are the variables that compose the vector *x* presented in (18).

However, as in most embedded systems, this equation must be discretized. Then, (21) shows the result of the discretization by the trapezoidal or *Tustin* method.

$$\begin{gathered} A_2(x[n] - 2x[n-1] + x[n-2]) + \\ A_1 dt(x[n] - x[n-1]) + A_0 dt^2 x[n] - \\ B_2(y[n] - 2y[n-1] + y[n-2]) - \\ B_1 dt(y[n] - y[n-1]) = dt^2 y[n] \end{gathered} \tag{20}$$

where *dt* is the simulation sampling step.

Therefore, based on the above equation, one can, through an input and output vector of a system similar to that shown in (19), estimate the parameters A_2, A_1, A_0, B_2, and B_1.

C. AIS Technique Implementation

The AIS was developed in a simulation software and followed the flowchart structure shown in Fig. 1, where each individual of the population represents a random input signal, starting from zero and oscillating randomly along its length. This signal is used to excite the estimated control plant, which, compared to the real one, returns the Objective Function (OF) of the algorithm.

The variable i_T is the current iteration and $i_{T_{MAX}}$ is the stop criteria. Since this paper aims to estimate the signal that best approximates the real control plant by the RLS method, the objective function here is to minimize the error between the responses of both plants. Thus, the obtained response in the original system is compared to the obtained one in the simulated plant through the mean square error between the signals.

The random signals (individuals) are created using a discrete approach. In order to create the signal, a matrix with pre-established dimensions is used. The higher the used matrix, the higher is the created signal level of detail, since each cell of the respective matrix represents a possible value for the signal. From the initial matrix, the neighbors of each cell are mapped. These neighbors are used to identify the possible paths to be taken.

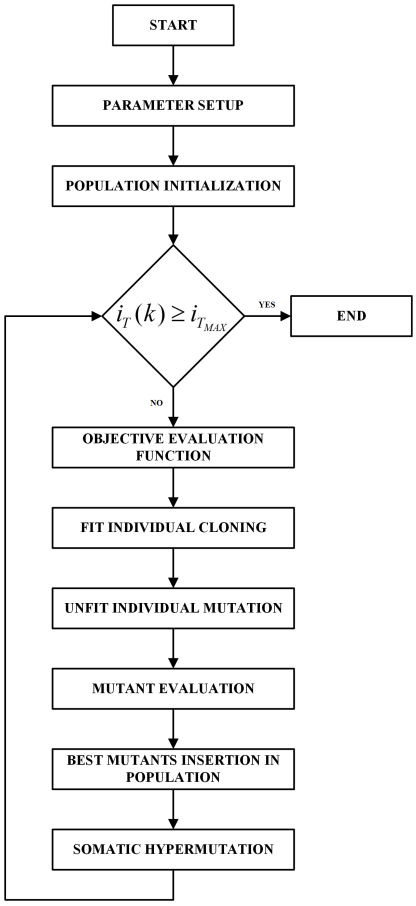

Figure 1. AIS algorithm flowchart.

Each cell can have a maximum of five neighbors, as the signal is sequential. However, in this approach, only three are used, as shown in Fig. 2.

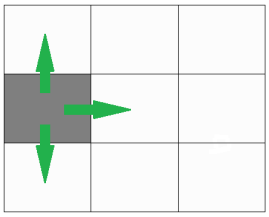

Figure 2. Neighbor cells diagram.

With the assembled neighbor matrix, one can randomly select a current cell neighbor to insert it as a new value in the signal being built. The process is repeated until it reaches the end of the matrix, presenting a result such as an example shown in Fig. 3.

Once assembled, the discrete signal goes through a manipulation, where each cell is transformed into a value between predetermined limits, both in amplitude and time. This manipulation causes the signal to be within a controlled range, which can be used to avoid amplitudes not allowed in the applied

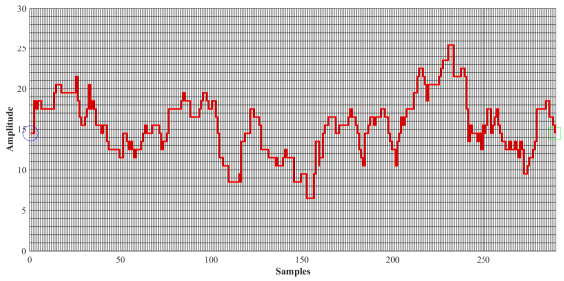

Figure 3. Discretized signal.

system. The result of signal manipulation can be seen in Fig. 4.

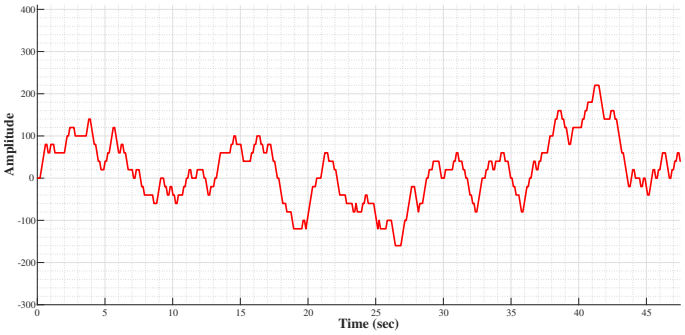

Figure 4. Time-varying signal.

IV. Tests and Results

The tests consisted in using the algorithm to estimate the signals to identify functions that represent the models of the control meshes of Euler angles of a quadrotor in a simulation software. For all tests, 50 generations and 30 individuals are used.

As previously mentioned, the angular control loop of a quadrotor can be represented by a second-order transfer function, with canonical form given by (17), where ω_n is the natural frequency of the system and ζ is the damping coefficient. Since all three control loops have the same characteristics, different values of ω_n and ζ were used on each test.

With values of ω and ζ used in [36], as shown in Table I, the AIS was applied to optimize the transfer function estimation by choosing a correct input signal.

TABLE I
Parameters ω and ζ.

Angle	ω	ζ
Roll	1	0.8
Pitch	1.5	0.95
Yaw	1.2	0.75

The result of the algorithm can be seen in Figs. 5, 6, and 7, and was obtained with the merit figures presented in Table II.

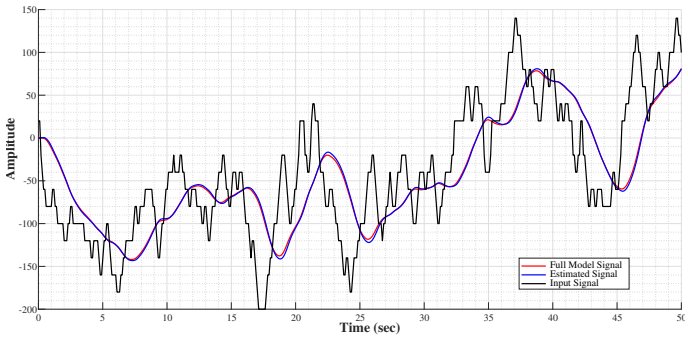

Figure 5. Optimized signal, estimated plant response, and original plant response for the roll angle control loop.

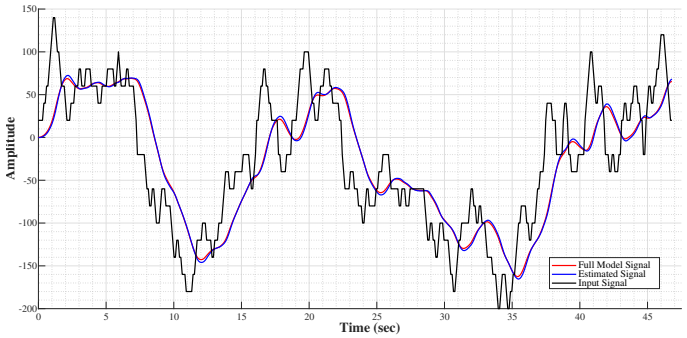

Figure 6. Optimized signal, estimated plant response, and original plant response for the pitch angle control loop.

TABLE II
MERIT FIGURES.

Attitude Angle	Number of Iterations	Simulation Time (s)	Mean Square Error
Roll	50	36.9331	0.0378
Pitch	50	32.7796	0.0559
Yaw	50	32.3309	0.0587

The estimated plant responses follow the shape of the original transfer function without presenting major errors. The estimated transfer functions of rolling, pitching, and yawing are given by (21), (22), and (23), respectively.

$$G(s) = \frac{0.001605s^2 - 0.09881s + 1}{0.9228s^2 + 1.501s + 1} \tag{21}$$

$$G(s) = \frac{0.001556s^2 - 0.0978s + 1}{0.3847s^2 + 1.169s + 1} \tag{22}$$

$$G(s) = \frac{0.001597s^2 - 0.09863s + 1}{0.6345s^2 + 1.151s + 1} \tag{23}$$

Since the constants that follow s^2 and s in the obtained transfer function numerator are very low and, thus, can be neglected, the values of ω and ζ are very close to those used in the algorithm. For the roll angle control loop, for instance,

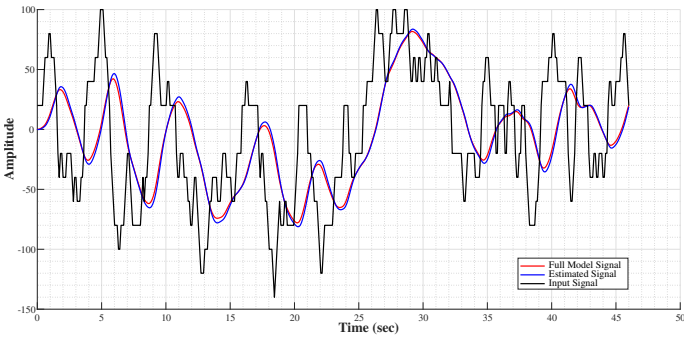

Figure 7. Optimized signal, estimated plant response, and original plant response for the yaw angle control loop.

the obtained values of ω and ζ were 1.0409 and 0.7813, respectively. Therefore, one can verify the effectiveness of the used method.

V. CONCLUSIONS

This paper proposed the implementation of an optimization technique based on Artificial Immunological Systems to the signal estimation that best provides the identification of an angular control loop of a quadrotor. The system was approximated by a second-order function using Recursive Least Square method.

The AIS optimization technique obtained a satisfactory result at the end of its execution, presenting in its response a rich enough signal for the transfer function estimation using RLS method. Furthermore, the algorithm did not require a large number of individuals and iterations to find a good signal. Consequently, the result is presented in reduced time.

Concerning the tests, it was observed that the estimated transfer functions presented a negligible error for most applications compared to the real plant, presenting a relatively low value of mean square error.

As future works, different methods and approaches can be implemented, such as used in [15], [16], [23], [39]–[42]. Another important works about optimization techniques to be followed are [43]–[45].

ACKNOWLEDGMENT

The authors thank INERGE, UFJF, CEFET-MG, CPFL and TBE for the financial support.

REFERENCES

[1] H. M. Khodr, Z. Vale, C. Ramos, and P. Faria, "Optimization techniques for power distribution planning with uncertainties: A comparative study," in *Power & Energy Society General Meeting, PES'09*, pp. 1–8, IEEE, 2009.

[2] S. Kirkpatrick, M. P. Vecchi, *et al.*, "Optimization by simmulated annealing," *science*, vol. 220, no. 4598, pp. 671–680, 1983.

[3] M. Dorigo and L. M. Gambardella, "Ant colony system: a cooperative learning approach to the traveling salesman problem," *IEEE Transactions on Evolutionary Computation*, vol. 1, no. 1, pp. 53–66, 1997.

[4] K. Leung, F. Cheong, and C. Cheong, "Generating compact classifier systems using a simple artificial immune system," *Transactions on Systems, Man, and Cybernetics. Part B: Cybernetics*, no. 5, pp. 1344–1356, 2007.

[5] Y. Chen, X. Wang, Q. Zhang, and C. Tang, "Unified artificial immune system," in *5th International Conference on Computational Intelligence and Communication Networks (CICN)*, pp. 617–621, Sept 2013.

[6] S. Forrest, A. S. Perelson, L. Allen, and R. Cherukuri, "Self-nonself discrimination in a computer," in *Computer Society Symposium on Research in Security and Privacy*, pp. 202–212, Ieee, 1994.

[7] L. N. Castro and F. J. Von Zuben, "The clonal selection algorithm with engineering applications," in *Proceedings of GECCO*, vol. 2000, pp. 36–39, 2000.

[8] L. N. Castro and F. J. Von Zuben, "An evolutionary immune network for data clustering," in *6th Brazilian Symposium on Neural Networks*, pp. 84–89, IEEE, 2000.

[9] J. Timmis, M. Neal, and J. Hunt, "Data analysis using artificial immune systems, cluster analysis and kohonen networks: some comparisons," in *International Conference on Systems, Man, and Cybernetics, (SMC'99)*, pp. 922–927, IEEE, 1999.

[10] J. Timmis, M. Neal, and J. Hunt, "An artificial immune system for data analysis," *Biosystems*, no. 1, pp. 143–150, 2000.

[11] J. Timmis and M. Neal, "A resource limited artificial immune system for data analysis," *Knowledge-Based Systems*, no. 3, pp. 121–130, 2001.

[12] M. Gong, L. Jiao, H. Du, and L. Bo, "Multiobjective immune algorithm with nondominated neighbor-based selection," *Evolutionary Computation*, no. 2, pp. 225–255, 2008.

[13] L. N. Castro and J. Timmis, "An artificial immune network for multimodal function optimization," in *Congress on Evolutionary Computation, (CEC'02)*, pp. 699–704, IEEE, 2002.

[14] C. A. C. Coello and N. C. Cortés, "Solving multiobjective optimization problems using an artificial immune system," *Genetic Programming and Evolvable Machines*, no. 2, pp. 163–190, 2005.

[15] L. M. Honório, M. Vidigal, and L. E. Souza, "Dynamic polymorphic agents scheduling and execution using artificial immune systems," in *International Conference on Artificial Immune Systems*, pp. 166–175, Springer, 2008.

[16] L. M. Honório, A. M. L. da Silva, D. A. Barbosa, and L. F. N. Delboni, "Solving optimal power flow problems using a probabilistic α-constrained evolutionary approach," *IET generation, transmission & distribution*, vol. 4, no. 6, pp. 674–682, 2010.

[17] D. Dasgupta and S. Forrest, "Artificial immune systems in industrial applications," in *2nd International Conference on Intelligent Processing and Manufacturing of Materials, (IPMM'99)*, pp. 257–267, IEEE, 1999.

[18] M. F. A. Gadi, X. Wang, and A. P. do Lago, "Credit card fraud detection with artificial immune system," in *Artificial immune systems*, pp. 119–131, Springer, 2008.

[19] H. Yang, M. Elhadef, A. Nayak, and X. Yang, "Network fault diagnosis: an artificial immune system approach," in *14th International Conference on Parallel and Distributed Systems, (ICPADS'08)*, pp. 463–469, IEEE, 2008.

[20] P. K. Harmer, P. D. Williams, G. H. Gunsch, and G. B. Lamont, "An artificial immune system architecture for computer security applications," *IEEE transactions on Evolutionary computation*, no. 3, pp. 252–280, 2002.

[21] R. Mehra, "Optimal input signals for parameter estimation in dynamic systems–survey and new results," *IEEE Transactions on Automatic Control*, vol. 19, no. 6, pp. 753–768, 1974.

[22] M. Gevers, L. Miskovic, D. Bonvin, and A. Karimi, "Identification of multi-input systems: variance analysis and input design issues," *Automatica*, vol. 42, no. 4, pp. 559 – 572, 2006.

[23] L. M. Honório, E. B. Costa, E. J. Oliveira, D. de Almeida Fernandes, and A. P. G. Moreira, "Persistently-exciting signal generation for optimal parameter estimation of constrained nonlinear dynamical systems," *ISA transactions*, 2018.

[24] V. F. Vidal, L. M. Honório, M. F. Santos, M. F. Silva, A. S. Cerqueira, and E. J. Oliveira, "UAV vision aided positioning system for location and landing," in *18th International Carpathian Control Conference (ICCC)*, pp. 228–233, IEEE, 2017.

[25] A. Gautam, P. B. Sujit, and S. Saripalli, "A survey of autonomous landing techniques for UAVs," in *International Conference on Unmanned Aircraft Systems (ICUAS)*, pp. 1210–1218, IEEE, 2014.

[26] M. Zuccolotto, L. Fasanotti, S. Cavalieri, and C. E. Pereira, "A distributed intelligent maintenance approach based on artificial immune systems," pp. 969–981, 2015.

[27] J. L. M. Amaral, *Sistemas imunológicos artificiais aplicados à detecção de falhas*. PhD thesis, PUC-Rio, 2006.

[28] J. Awrejcewicz, *Modeling, Simulation and Control of Nonlinear Engineering Dynamical Systems*. Springer, 2009.

[29] L. Dai and R. N. Jazar, *Nonlinear Approaches in Engineering Applications 2*. Springer, 2012.

[30] T. I. Fossen, "Mathematical models for control of aircraft and satellites," *Department of Engineering Cybernetics Norwegian University of Science and Technology*, 2011.

[31] F. C. Ferreira, M. F. Santos, and V. B. Schettino, "Computational vision applied to mobile robotics with position control and trajectory planning: Study and application," in *19th International Carpathian Control Conference (ICCC)*, IEEE, 2018.

[32] R. W. Beard, "Quadrotor dynamics and control," *Brigham Young University*, 2008.

[33] M. F. Silva, A. C. Ribeiro, M. F. Santos, M. J. Carmo, L. M. Honório, E. J. Oliveira, and V. F. Vidal, "Design of angular PID controllers for quadcopters built with low cost equipment," in *20th International Conference on System Theory, Control and Computing (ICSTCC)*, pp. 216–221, IEEE, Oct 2016.

[34] M. F. Santos, L. M. Honório, E. B. Costa, E. J. Oliveira, and J. P. P. G. Visconti, "Active fault-tolerant control applied to a hexacopter under propulsion system failures," in *19th International Conference on System Theory, Control and Computing (ICSTCC)*, pp. 447–453, Oct 2015.

[35] M. F. Santos, V. S. Pereira, A. C. Ribeiro, M. F. Silva, M. J. Carmo, V. F. Vidal, L. M. Honório, A. S. Cerqueira, and E. J. Oliveira, "Simulation and comparison between a linear and nonlinear technique applied to altitude control in quadcopters," in *18th International Carpathian Control Conference (ICCC)*, pp. 234–239, IEEE, 2017.

[36] M. F. Silva, A. C. Ribeiro, M. F. Santos, M. J. Carmo, L. M. Honório, E. J. Oliveira, and V. F. Vidal, "Design of angular PID controllers for quadcopters built with low cost equipment," in *20th International Conference on System Theory, Control and Computing (ICSTCC)*, pp. 216–221, IEEE, 2016.

[37] A. A. Silva, "Determinação de órbitas com o GPS através de mínimos quadrados recursivo com rotações de givens, universidade estadual paulista UNESP," 2001.

[38] G. J. Bierman and C. L. Thornton, "Numerical comparison of kalman filter algorithms: Orbit determination case study," *Automatica n. 13*, no. 1, pp. 23–35, 1977.

[39] L. M. Honório, D. A. Barbosa, E. J. Oliveira, P. A. N. Garcia, and M. F. Santos, "A multiple kernel classification approach based on a quadratic successive geometric segmentation methodology with a fault diagnosis case," *ISA transactions*, 2018.

[40] M. F. Silva, A. S. Cerqueira, V. F. Vidal, L. M. Honório, M. F. Santos, and E. J. Oliveira, "Landing area recognition by image applied to an autonomous control landing of VTOL aircraft," in *18th International Carpathian Control Conference (ICCC)*, pp. 240–245, IEEE, 2017.

[41] M. M. Machado, A. J. Carvalho, M. F. Santos, and J. R. de Carvalho, "Case study: Level and temperature multivariable control and design via arduino through control loop decoupling," in *19th International Carpathian Control Conference (ICCC)*, IEEE, 2018.

[42] E. J. Oliveira, L. M. Honório, A. H. Anzai, L. W. Oliveira, and E. B. Costa, "Optimal transient droop compensator and PID tuning for load frequency control in hydro power systems," *International Journal of Electrical Power & Energy Systems*, vol. 68, pp. 345–355, 2015.

[43] L. C. Gonçalves, M. F. Santos, R. J. F. de Sá, J. L. da Silva, H. B. Rezende, *et al.*, "Development of a PI controller through an ant colony optimization algorithm applied to a SMAR® didactic level plant," in *19th International Carpathian Control Conference (ICCC)*, IEEE, 2018.

[44] F. F. Panoeiro, M. F. Santos, D. C. Silva, J. L. Silva, and M. J. Carmo, "PI controller tuned by bee swarm for level control systems," in *19th International Carpathian Control Conference (ICCC)*, IEEE, 2018.

[45] J. M. S. Ribeiro, M. F. Santos, M. J. Carmo, and M. F. Silva, "Comparison of PID controller tuning methods: analytical/classical techniques versus optimization algorithms," in *18th International Carpathian Control Conference (ICCC)*, pp. 533–538, IEEE, 2017.